Calculation of exchange constants of the Heisenberg model in plane-wave-based methods using the Green's function approach

Dm. M. Korotin,[1,*] V. V. Mazurenko,[2] V. I. Anisimov,[1,2] and S. V. Streltsov[1,2,†]

[1]*Institute of Metal Physics, S.Kovalevskoy St. 18, 620990 Yekaterinburg, Russia*

[2]*Department of Theoretical Physics and Applied Mathematics, Ural Federal University, Mira St. 19, 620002 Yekaterinburg, Russia*

(Received 11 January 2015; revised manuscript received 7 April 2015; published 4 June 2015)

An approach to compute exchange parameters of the Heisenberg model in plane-wave-based methods is presented. This calculation scheme is based on the Green's function method and Wannier function projection technique. It was implemented in the framework of the pseudopotential method and tested on such materials as NiO, FeO, Li_2MnO_3, and $KCuF_3$. The obtained exchange constants are in a good agreement with both the total energy calculations and experimental estimations for NiO and $KCuF_3$. In the case of FeO our calculations explain the pressure dependence of the Néel temperature. Li_2MnO_3 turns out to be a Slater insulator with antiferromagnetic nearest-neighbor exchange defined by the spin splitting. The proposed approach provides a unique way to analyze magnetic interactions, since it allows one to calculate orbital contributions to the total exchange coupling and study the mechanism of the exchange coupling.

DOI: 10.1103/PhysRevB.91.224405 PACS number(s): 75.10.−b, 31.15.A−

I. INTRODUCTION

Magnetic interactions are in the focus of theoretical and experimental investigations of many modern materials. Depending on the nature and localization of the magnetic moments, one can use different model Hamiltonians to describe the magnetic properties of the system. In the case of the localized magnetic moments, the spin-Hamiltonian approach based on the solution of the Heisenberg model can be used. The corresponding Heisenberg Hamiltonian has the form

$$H_{\text{Heis}} = \sum_{\langle ij \rangle} J_{ij} \hat{\mathbf{S}}_i \hat{\mathbf{S}}_j, \tag{1}$$

where J_{ij} is the isotropic exchange interaction parameters. One can also use different extensions of the Heisenberg model taking into account symmetric and antisymmetric parts of the anisotropic exchange coupling [1–3]. Within the spin-Hamiltonian approach the problem of realistic description of the magnetic properties is reduced to the problem of unambiguous determination of the exchange interactions by taking electronic structure and chemical bonding into account. It can be done on different levels and by using different means.

One of the most popular approaches for *ab initio* investigation of solids is density functional theory (DFT). There are a few methods to estimate exchange constants J_{ij} within DFT, i.e., to map the results of the DFT calculations onto the Heisenberg model.

The most direct, and popular way to calculate J_{ij} is to calculate the total energies of the $N + 1$ magnetic configurations, where N is the number of different exchange constants [4–6]. Despite the robustness of this approach, it has several serious drawbacks: (1) a number of different magnetic configurations have to be calculated for complicated systems; (2) all configurations must use the same magnetic moments (important for the materials close to itinerant regime); and (3) the result is purely a number, which is hard to analyze, i.e., understanding which orbitals contribute the most and what mechanism of exchange coupling (direct-exchange, superexchange, double-exchange, etc.) is present.

To overcome these shortcomings the Green's function method [7–9] can be utilized. Using DFT and Heisenberg model, it produces analytical expressions for the changes in the total energy with respect to small spin rotations. This approach allows one not only to obtain all the exchange constants from the calculation of a single magnetic configuration, but also to find contributions to the total exchange coupling coming from different orbitals (e.g., $J_{xy/xy}$, J_{xy/x^2-y^2}, etc.). Moreover, this method can easily be generalized to calculate the anisotropic part of the exchange Hamiltonian [10].

Previously, the Green's function approach was formulated for localized orbitals methods, e.g., linear muffin-tin orbitals (LMTO) method [11] or linear combination of atomic orbitals (LCAO) [12,13]. However, modern high-precision schemes of band structure calculations are mostly based on the methods, which use a plane-wave-type basis. They are the full-potential (linearized) augmented plane-wave (L)APW [14] and pseudopotential [5] methods. As a result, a straightforward realization of the Green's function method becomes impossible within plane-wave approaches and all its advantages cannot be used in the modern *ab initio* DFT codes without direct definition of a localized basis set.

In the present paper we show how the Green's function approach can be adapted for the plane-wave-based methods using the Wannier functions formalism. We implemented this calculation scheme in the pseudopotential Quantum-ESPRESSO code [15] and report the results concerning the magnetic interactions in NiO, FeO, Li_2MnO_3, and $KCuF_3$.

II. METHOD

Following Ref. [8], we used classical analog of Eq. (1) with spins substituted by the unit vectors $\mathbf{e}_i$ pointing in the direction of the ith site magnetization:

$$H = \sum_{\langle ij \rangle} J_{ij} \mathbf{e}_i \mathbf{e}_j. \tag{2}$$

*dmitry@korotin.name

†streltsov@imp.uran.ru

The value of the exchange constants for the conventional classical Heisenberg model (with spins, not unit vectors) can be obtained with a proper renormalization.

The power of the Green's function method is in the application of the local force theorem (see, e.g., Ref. [16]). When the spins experience rotations over a small angle $\delta\phi$, the resulting change in the total energy in the DFT can be calculated via the local force theorem [8]. This can only be done if the Hamiltonian of the system is defined in a localized orbitals basis set (otherwise, it is not clear what parts of the Hamiltonian have to be rotated). The result of the rotation is compared with a similar procedure performed for the spin-Hamiltonian Eq. (2), which allows us to derive an analytical expression for the exchange integrals Eq. (8). The major difficulty in the application of this approach to the modern plane-wave-based calculation schemes is the absence of the localized basis set in these methods. We propose to use the Wannier functions (WF) projection procedure to avoid this restriction and show its realization for the pseudopotential method.

It is important to note that the Heisenberg model is defined for localized spin moments. Therefore, the basis set with the most localized orbitals is the best for a mapping of the DFT results on the Heisenberg model. Hence, the maximally localized Wannier functions [17] represent the most natural choice for such a mapping. Technically, the localization degree and the symmetry of such wavefunctions can be controlled in the projection procedure. One of the most widespread procedures is an enforcement of maximum localization of WF [18]. The second [19] is a constraint for the WF symmetry to be the same as the symmetry of pure atomic d orbitals. In the present paper, the second type of projection procedure is used.

The WFs were generated as projections of the pseudoatomic orbitals $|\phi_{n\mathbf{k}}\rangle = \sum_{\mathbf{T}} e^{i\mathbf{kT}}|\phi_n^{\mathbf{T}}\rangle$ onto a subspace of the Bloch functions $|\Psi_{\mu\mathbf{k}}\rangle$ (the detailed description of WFs construction procedure within pseudopotential method is given in Ref. [20]):

$$\left|W_n^{\mathbf{T}}\right\rangle = \frac{1}{\sqrt{N_{\mathbf{k}}}}\sum_{\mathbf{k}}|W_{n\mathbf{k}}\rangle e^{-i\mathbf{kT}}, \tag{3}$$

where

$$|W_{n\mathbf{k}}\rangle \equiv \sum_{\mu=N_1}^{N_2}|\Psi_{\mu\mathbf{k}}\rangle\langle\Psi_{\mu\mathbf{k}}|\phi_{n\mathbf{k}}\rangle. \tag{4}$$

Here $\mathbf{T}$ is the lattice translation vector. The resulting WFs have the symmetry of the atomic orbitals ϕ_n and describe the electronic states that form energy bands numbered from N_1 to N_2.

The matrix elements of the one-electron Hamiltonian in the reciprocal space are defined as

$$H^{\mathrm{WF}}_{nm,\sigma}(\mathbf{k}) = \langle W_{n\mathbf{k}}|\left(\sum_{\mu=N_1}^{N_2}|\Psi_{\mu\mathbf{k}}\rangle\varepsilon^{\sigma}_{\mu}(\mathbf{k})\langle\Psi_{\mu\mathbf{k}}|\right)|W_{m\mathbf{k}}\rangle, \tag{5}$$

where $\varepsilon^{\sigma}_{\mu}(\mathbf{k})$ is the eigenvalue of the one-electron Hamiltonian for band μ and spin σ.

Such a Hamiltonian matrix is produced as a result of the WF projection procedure at the end of the self-consistent cycle in the spin-polarized DFT or DFT+U calculations.

This matrix in the $H^{\mathrm{WF}}_{mm',ij,\sigma}$ form (where m and m' numerate orbitals on ith and jth sites, respectively) can be used for the intersites Green's function calculation at every $\mathbf{k}$ point in reciprocal space:

$$G^{mm'}_{ij,\sigma}(\varepsilon,\mathbf{k}) = \left[\varepsilon + E_F - H^{\mathrm{WF}}_{mm',ij,\sigma}(\mathbf{k})\right]^{-1}, \tag{6}$$

where E_F is the Fermi energy. The site indexes i and j run through atoms within the primitive cell by default; however, the intersite Green's function between any two atoms of the lattice sites i' and j' could be obtained via integration over Brillouin zone (BZ):

$$G^{mm'}_{i'j',\sigma}(\varepsilon) = \int_{\mathrm{BZ}} G^{mm'}_{ij,\sigma}(\varepsilon,\mathbf{k})e^{i\mathbf{k}[(\mathbf{R}_{i'}-\mathbf{R}^0_i)-(\mathbf{R}_{j'}-\mathbf{R}^0_j)]}d\mathbf{k}, \tag{7}$$

where $G^{mm'}_{ij,\sigma}(\mathbf{k})$ is the intersite Green's function of the primitive cell for given $\mathbf{k}$ point, $\mathbf{R_{i'}}$ is the position of atom i' in the lattice, and $\mathbf{R^0_i}$ is the position of the same atom within the primitive cell.

The resulting $G^{mm'}_{i'j',\sigma}(\varepsilon)$ is used in the analytic expression for the exchange integrals as obtained in the Green's function method [8]:

$$J_{ij} = -\frac{1}{2\pi}\int_{-\infty}^{E_F} d\varepsilon \sum_{\substack{mm'\\ m''m'''}} \mathrm{Im}\left(\Delta^{mm'}_i G^{m'm''}_{ij,\downarrow}\Delta^{m''m'''}_j G^{m'''m}_{ji,\uparrow}\right), \tag{8}$$

where $G^{mm'}_{ji,\uparrow}$ ($G^{mm'}_{ij,\downarrow}$) is the real-space intersite Green's function for spin-up (-down) obtained in Eq. (7) and

$$\Delta^{mm'}_i = \int_{\mathrm{BZ}}\left[H^{mm'}_{ii,\uparrow}(\mathbf{k}) - H^{mm'}_{ii,\downarrow}(\mathbf{k})\right]d\mathbf{k}. \tag{9}$$

The proposed scheme allows us to compute per-orbital contribution to the exchange interaction between two atoms. Without spin-orbit coupling the $\Delta^{mm'}_i$ matrix is diagonal in the spin subspace, but it is not necessarily diagonal in the orbital subspace. However, one may always transform $\Delta^{mm'}_i$ to the diagonal form (e.g., changing the global coordinate system of the crystal to the local one, when axes are directed to the ligands; or simply diagonalizing onsite Hamiltonian matrix in the WF basis set):

$$\Delta^{mm'}_i = \sum_k T^{mk}_i \tilde{\Delta}^{kk}_i \left(T^{km'}_i\right)^*. \tag{10}$$

Then Eq. (8) can be rewritten as

$$J^{kk'}_{ij} = -\frac{1}{2\pi}\int_{-\infty}^{E_F} d\varepsilon \sum_{kk'} \mathrm{Im}\left(\tilde{\Delta}^{kk}_i \tilde{G}^{kk'}_{ij,\downarrow}\tilde{\Delta}^{k'k'}_j \tilde{G}^{k'k}_{ji,\uparrow}\right), \tag{11}$$

where

$$\tilde{G}^{kk'}_{ij,\sigma} = \sum_{mm'} T^{km}_i \tilde{G}^{mm'}_{ij,\sigma}\left(T^{m'k'}_j\right)^*. \tag{12}$$

Equation (11) allows us to calculate exchange coupling between the kth orbital on site i and the k'th orbital on site j.

In the end of this section we would like to stress that one should carefully choose the orbital set used in the projection procedure. First of all, technically it should be the set and the energy window for the projection, which give the band structure identical (or close to) initial. Second, this set should be physically reasonable. For example, if one deals with compounds (like NiO and $KCuF_3$), where the main exchange mechanism is expected to be superexchange via, e.g., ligand p

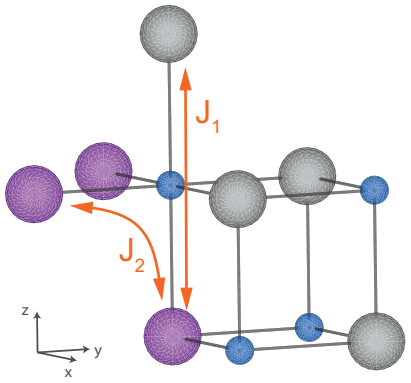

FIG. 1. (Color online) Schematic view of the NiO crystal structure. The blue spheres denote oxygen ions, while the gray and magenta spheres denote two magnetic types of Ni. The figure was drawn using VESTA [21] software.

orbitals, then corresponding states have to be included in the projection procedure. This, in turn, provides an additional tool to study the exchange paths and mechanism of the magnetic coupling, whether it is due to direct- or superexchange.

III. RESULTS AND DISCUSSION

A. NiO

NiO is one of the typical systems on which different calculation schemes are tested. It is a charge-transfer insulator with a band gap ∼4 eV [22] and local magnetic moment of 1.77 μ_B [23]. NiO crystallizes in the rocksalt (NaCl) structure and exhibits an antiferromagnetic ordering of type-II fcc (AFM II-type) [24], with planes of opposite spins being repeated in alternating order along [111]; see Fig. 1. This type of magnetic ordering is due to the strong next-nearest-neighbor (nnn) coupling between nickel ions via oxygen's $2p$ shell. The Néel temperature is $T_N = 523$ K [25].

Since accounting for strong electronic correlations is crucial in the case of NiO [26], we used the LSDA+U method [27] for the calculation of electronic and magnetic properties. The onsite Coulomb repulsion and intra-atomic Hund's rule exchange parameters were chosen to be $U = 8.0$ eV and $J_H = 0.9$ eV, respectively [26]. We used the Perdew-Zunger exchange-correlation potential [28], 45 and 360 Ry for the charge density and kinetic energy cutoffs, and 512 **k** points in the Brillouin zone (BZ). The unit cell consists of two formula units to simulate AFM II-type.

First of all, we have calculated the dominating exchange interactions for the Heisenberg model Eq. (1) between second-nearest neighbors, J_1 (see Fig. 1), using conventional total energy technique, and obtained $J_1 = 18.8$ meV, which agrees extremely well with experimental estimation of $J_1 = 19.0$ meV [29].

The small effective Hamiltonian used for the Green's function calculation according to Eq. (6) was obtained by the Wannier function projection procedure as described in Sec. II. The Wannier functions were constructed as a projection of the Ni $3d$ and O $2p$ pseudoatomic orbitals onto subspace of Bloch functions defined by the 16 energy bands, which predominantly have the Ni $3d$ and O $2p$ character: 2 formula units × (5 Ni $3d$ plus 3 O $2p$ orbitals) = 16.

The exchange constants calculated by the Green's function method are $J_1 = 18.9$ meV and $J_2 = -0.4$ meV, which agree with both the total energy and experimental estimations. Moreover, they allow us to perform an analysis of partial contributions from different orbitals. An orbital-resolved matrix (in meV) for the largest exchange interaction J_1 between the next-nearest neighbors along z (c) direction [calculated according to Eq. (11)] is given as

$$J_1^{mm'} = \begin{pmatrix} -18.9 & 0 & 0 & 0 & 0 \\ 0 & 0 & 0 & 0 & 0 \\ 0 & 0 & 0 & 0 & 0 \\ 0 & 0 & 0 & 0 & 0 \\ 0 & 0 & 0 & 0 & 0 \end{pmatrix}. \quad (13)$$

Here the following order of the $3d$ orbital is used: $3z^2 - r^2$, zx, zy, $x^2 - y^2$, xy; and the axes of the coordinate system are shown in Fig. 1. Thus, one may see that the exchange coupling between the next-nearest neighbors is due to overlap between $3z^2 - r^2$ orbitals centered on different sites. This is the 180° superexchange interaction via the $2p_z$ orbital of the oxygen sitting between two Ni ions in the z (c) direction, which has to be strong and AFM according to Goodenough-Kanamori-Anderson rules [30]. In contrast, the exchange interaction between nearest neighbors, J_2, occurs via two orthogonal p orbitals and is expected to be weak and ferromagentic (FM) [30].

The imaginary parts of the onsite and intersite Green's functions are shown in Fig. 2. The intersite Green's function (lower panel) corresponds to the strongest 180° exchange coupling, J_1. The exchange constants, defined in Eq. (8), is the energy integral of two Green's functions and two Δ functions, which do not depend on ε. Therefore, it is important to explore an energy dependence of the Green's function.

One can see that the imaginary part of the onsite Green's function (upper panel) doesn't change its sign over the entire energy interval and after normalization the function is exactly equal to density of electronic states. The energy integral of the imaginary part of the onsite Green's function up to the Fermi level gives the total number of electrons on corresponding orbitals. This value is predictable and slight changes of the onsite Green's function peak positions and widths will not change the resulting number of electrons significantly.

The intersite Green's function, shown in the lower panel of Fig. 2, changes its sign several times. It means that in a general case the energy integral up to the Fermi level has an unpredictable sign and the value strongly depends on the Green's function peak positions and widths, i.e., on band structure calculation results.

B. $KCuF_3$

$KCuF_3$ is renowned due to its orbital order, which defines its magnetic properties. The single hole in the e_g subshell of Cu^{2+} ion (its electronic configuration is $3d^9$) is localized on the alternating $z^2 - x^2$ and $z^2 - y^2$ orbitals present in the ab plane (i.e., antiferro-orbital order), which results in the weak ferromagnetic coupling in this plane. In contrast, there is a ferro-orbital ordering in the c direction, which leads to a strong

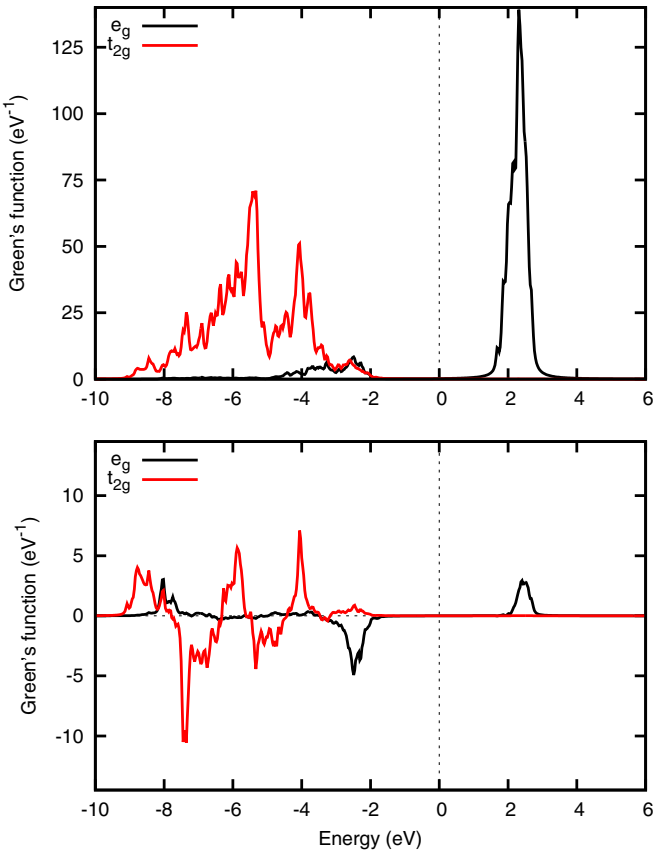

FIG. 2. (Color online) Imaginary part of the spin-up onsite (upper panel) Green's function of Ni ion and intersite (lower panel) Green's function for the pair of the Ni ions along c axis (i.e., corresponding to J_1). The Green's function for the e_g states is shown by solid black curve, and for the t_{2g} states by the solid red curve. Zero energy corresponds to the Fermi level.

antiferromagnetic interaction along this axis. As a result in the essentially three-dimensional (3D) crystal one may observe the formation of nearly ideal one-dimensional antiferromagnetic Heisenberg chains [31,32].

The compound has a distorted cubic perovskite crystal structure (shown in Fig. 3) with space group $I4/mcm$. The copper ions have octahedral fluorine surrounding. These octahedra are elongated along one of the directions. At room temperature, there are two different structural polytypes with antiferro (a-type) and ferro-like (d-type) stacking of the ab planes along the c axis [33].

Altogether, the electronic and structural properties of $KCuF_3$ have previously been intensively studied by employing density functional theory and its extensions like the DFT+U approach [26]. The DFT+U calculations led to a correct insulating ground state with the spin and orbital ordering [34–36] that are in agreement with experimental data. We used the GGA+U approach as a starting point for the exchange interaction parameters calculation.

For the density functional calculations, we used the Perdew-Burke-Ernzerhof [37] GGA exchange-correlation functional together with Vanderbilt ultrasoft pseudopotentials. We set the kinetic energy cutoff to 50 Ry (400 Ry) for the plane-wave expansion of the electronic states (core-augmentation charge).

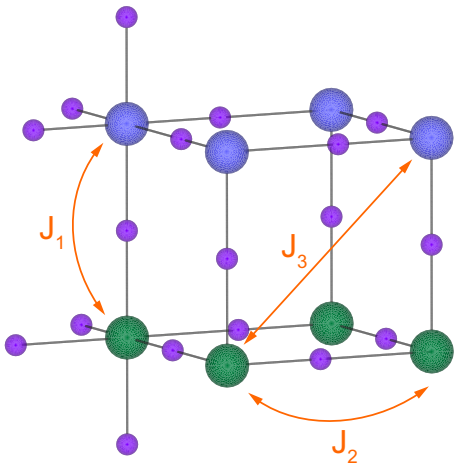

FIG. 3. (Color online) Schematic view of the KCuF3 crystal structure. The blue and green spheres denote Cu ions of two different types, while the violet spheres denote F ions. The potassium ion in the center of the cell is not shown for clarity.

The self-consistent calculation was performed with the $4 \times 4 \times 4$ Monkhorst-Pack $\mathbf{k}$-point grid. We set the effective onsite Coulomb interaction as $U_{\text{eff}} = U - J_H = 6.6$ eV [36]. To reproduce the magnetic and orbital ordering of the polytype a, we used a cell containing four formula units.

The basis of the WFs has a dimension of 56. It includes 20 Cu-d-like WFs (5 functions for every Cu site) and 36 F-p-like WF. We generated the Cu WF using a linear combination of pseudoatomic Cu-d orbitals to obtain a more clear physical basis for the Green's function formalism.

The strongest exchange interaction was found to be between nearest Cu ions along the c axis, $J_1 = 17$ meV (antiferromagnetic). As it was mentioned above, this is because of the ferro-orbital order in this direction, given by $J_1 \sim t^2/U$ (where t is corresponding hopping integral). The calculated value agrees with different experimental estimations of J_1, which was found be 16.1 meV [38] using analysis of the specific heat data, 16.2 meV [39] based on the temperature dependence of the magnetic susceptibility, and 17 meV [40] or 17.5 meV [41] in neutron measurements.

The exchange coupling in the ab plane, given by $J_2 \sim t^2 J_H/U^2$, has to be much weaker, since there is an antiferro-orbital order. Our calculations give $J_2 = 0.5$ meV. The additional "diagonal" exchange, J_3, was estimated to be -1 meV.

The onsite and intersite Green's functions for $KCuF_3$ are shown in Fig. 4. The main contribution to exchange interaction in c direction comes from the overlap between the similar WFs centered on different Cu ions (i.e., $z^2 - y^2/z^2 - y^2$ or $z^2 - x^2/z^2 - x^2$).

C. FeO

FeO together with NiO is one of the most studied monoxides. The crystal structure of these oxides is quite similar and shown in Fig. 1 (there are small rhombohedral distortions in the magnetically ordered phase of FeO), but magnetic properties of FeO strongly depend on the amount

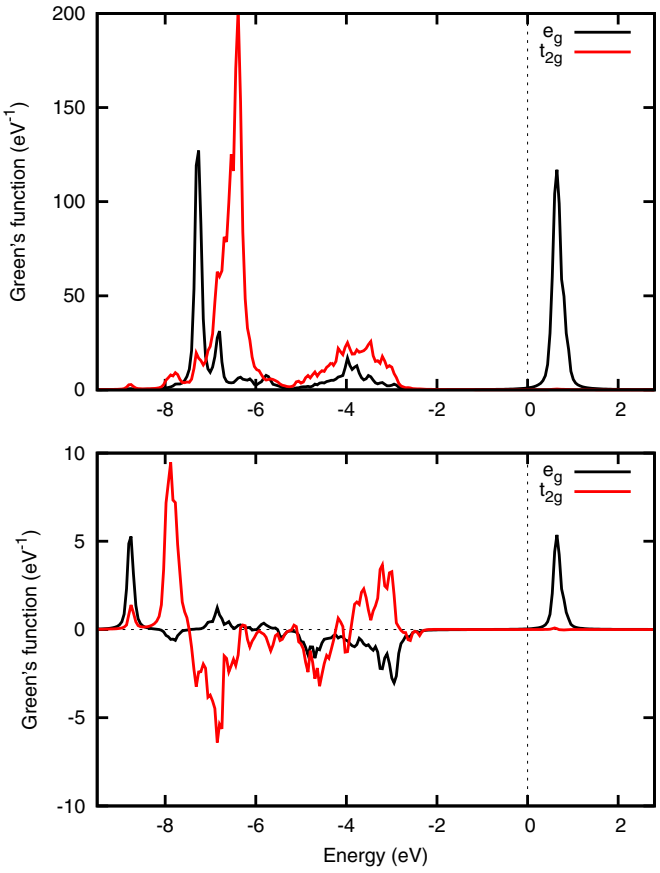

FIG. 4. (Color online) Imaginary part of the spin-down onsite (upper panel) Green's function of Cu ion and intersite (lower panel) Green's function for two Cu ions corresponding to J_1. The Green's function for e_g states is shown by the solid black line, for t_{2g} states by the solid red one. Zero energy corresponds to the Fermi level.

of defects in samples. The ordered moment changes from 3.2 to 4.5 μ_B, while Néel temperature T_N is ∼200 K (FeO orders in the AFM II-type structure; the same as NiO) [42]. Due to geophysical importance of FeO the investigations were mostly concentrated on the pressure dependence of its magnetic properties. Possible presence of the pressure-driven spin-state transition was studied by different methods starting from the conventional DFT calculations to more elaborated methods based on the dynamical mean-field theory (DMFT) [43–45]. However, in addition to this transition there is also unconventional change of T_N with the pressure [46]. Thorough study of this effect in a wide pressure range is beyond the scope of the present paper, but we estimated the change of the Néel temperature for moderate pressures.

We used experimental crystal structure for zero pressure [42], and optimized it (keeping the symmetry) for the pressure of 15 GPa. Standard PBE pseudopotentials from the Quantum-ESPRESSO pseudopotentials library were used for the self-consistent ground-state calculation. The plane-wave energy cutoff value was set to 45 Ry. Integration over the reciprocal cell was performed on $6 \times 16 \times 16$ regular **k**-points grid. The Hubbard's parameters $U = 5$ eV and $J_H = 0.9$ eV were calculated by one of us for FeO in the same pseudopotential code previously [45]. The WF basis consists of 16 Wannier functions. It includes states with Fe-d and O-p orbitals symmetry for two formula units.

The second nearest-neighbor exchange coupling (see Fig. 1) was found to be $J_1 = 2.1$ meV for the Heisenberg model written in Eq. (1). In the mean-field approximation the Néel temperature for the fcc lattice and AFM of II-type can be estimated as $6J_1\frac{1}{3}S(S+1)$, which gives $T_N \sim 300$ K, while experimental $T_N^{\exp} \sim 200$ K. This is a common feature of the mean-field theories to overestimate the transition temperature in 1.5–2 times (e.g., the situation in NiO is rather similar; if one would even use experimental $J_1 = 19$ meV, the Néel temperature will be strongly overestimated). What is more representative is the ratio between T_N for different pressures. Experimentally, $T_N^{P=15}/T_N^{P=0} \approx 1.45$ [46], while theoretically we obtained $T_N^{P=15}/T_N^{P=0} = 1.4$. Thus, one doesn't need to use such a sophisticated technique as DMFT to describe pressure dependence of the Néel temperature in FeO (at least for moderate pressures), which can be explained by the modification of average Fe-O-Fe distance. Indeed, in the Mott-Hubbard systems the superexchange between half-filled orbitals is defined by effective hopping parameter $\tilde{t}_{dd}$ via ligand $2p$ orbitals [30],

$$J \sim \frac{\tilde{t}_{dd}^2}{U}, \tag{14}$$

and $\tilde{t}_{dd} \sim \frac{t_{pd}^2}{\Delta_{\mathrm{CT}}}$, where Δ_{CT} is the charge-transfer energy [47] and t_{pd} is the hopping between ligand p and metal d orbitals. Since this hopping scales as $t_{pd} \sim 1/d^{7/2}$ [13], where d is the distance between ligand and transition metal ion, then

$$\frac{T_N^{P=15}}{T_N^{P=0}} = \left(\frac{d_{\text{Fe-O}}^{P=0}}{d_{\text{Fe-O}}^{P=15}}\right)^{14}. \tag{15}$$

Such a crude estimation surprisingly works quite well. According to our GGA calculations going from zero to 15 GPa pressure $d_{\text{Fe-O}}$ changes on 2.7%. Then according to Eq. (15), $\frac{T_N^{P=15}}{T_N^{P=0}} = 1.45$, exactly as observed experimentally [46].

D. Li_2MnO_3

Compounds with general formula A_2BO_3, where A is an alkali metal, Li or Na, and B is a metal have layered crystal structure with B ions forming honeycomb lattice; see Fig. 5. They attract much attention not only due to possible technological application as battery cathode materials [48], but also represent special interest for the fundamental science. For example, Na_2IrO_3 is considered as a possible realization of the Kitaev model [49], while Li_2RuO_3 shows unusual valence bond liquid phase at high temperatures [50] and spin-gapped state below 540 K (at least in polycrystalline samples) [51,52]. In contrast to these systems in Li_2MnO_3 the long-range antiferromagnetic state is formed at $T_N = 36$ K with all Mn neighbors in the ab plane ordered AFM [53]. This result is rather unexpected, since in the 90° Mn-O-Mn geometry one might expect strong FM interaction between half-filled t_{2g} and empty e_g orbitals of Mn^{4+} ions [30,53,54].

We performed GGA and GGA+U calculations of the exchange parameters in Li_2MnO_3 using Perdew-Burke-Ernzerhof [37] exchange-correlation potential. The crystal

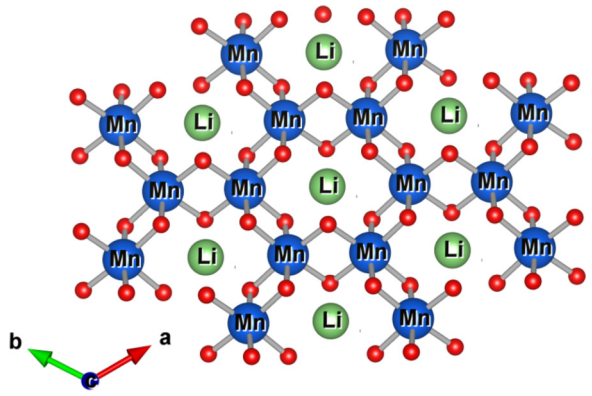

FIG. 5. (Color online) Crystal structure of Li_2MnO_3. Mn ions, shown by blue balls, are in octahedral surrounding of the O ions (red balls) and form honeycomb lattice, with Li (green balls) in the center of the honeycombs. These 2D hexagonal planes are stacked in the c direction with Li ions in between.

structure was taken from Ref. [53] for $T = 6$ K. The magnetic structure is AFM G-type, when all neighboring Mn are AFM coupled [53]. The kinetic energy cutoff was chosen to be 45 Ry (450 Ry) for the plane-wave expansion of the electronic states (core-augmentation charge) and we used 64 **k** points for the integration over the BZ.

The magnetic moments on Mn ions in the GGA approach were found to be 2.5 μ_B, which is consistent with 4+ oxidation state. The total and partial DOS are shown in Fig. 6. This is the feature of the Mn^{4+} ion with the half-filled t_{2g} subshell (electronic configuration $3d^3$), that the spin splitting (i.e., the splitting between spin-majority and spin-minority subbands) is quite large and therefore already magnetic GGA calculation gives insulating ground state with the band gap 1.9 eV. On the one hand, this is much larger than experimental activation energy $\Delta \sim 0.7$ eV deduced from the resistivity measurements [53], which, however, cannot be considered as a direct and precise way to estimate the band gap. On the other hand, this strongly suggests that the Hubbard correction, U, is not that

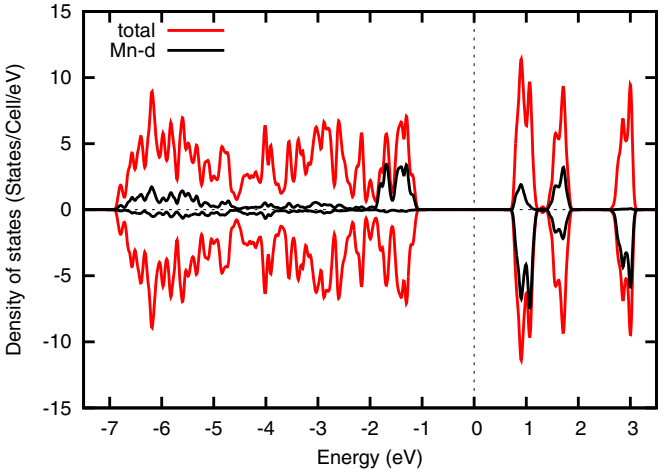

FIG. 6. (Color online) Spin-polarized density of electronic states for Li_2MnO_3 obtained in the magnetic GGA calculation. Zero energy corresponds to the Fermi level.

important for the descriptions of the top of the valence and the bottom of the conduction bands. Indeed, many other Mn oxides can be described by the LSDA or GGA methods without account of any Hubbard correlations [55–58].

Our GGA+U calculation shows that even quite large $U = 4.5$ eV only slightly increases the value of the band gap (on 0.3 eV), which shows that the band gap is indeed defined by the spin splitting (as clearly seen from Fig. 6) and not by the Coulomb correlations. Therefore, the use of the GGA approximation seems to be plausible for the description of the magnetic properties of Li_2MnO_3. This additionally allows us to test the Green's function approach for the calculation of the exchange constants without Hubbard's U.

We found that in the GGA approximation exchange coupling between nearest neighbors is $J = 23$ K (AFM) for the Heisenberg model defined in Eq. (1). In the mean-field approximation this gives Curie-Weiss temperature $\theta_{\mathrm{GGA}} = 87$ K. This is again somewhat larger than experimental $\theta_{\mathrm{exp}} \sim 50$–$60$ K [53], but it agrees with what one may expect from the mean-field theory. An account of the onsite Coulomb repulsion in the GGA+U calculation leads to gradual growth of the FM component and results in total exchange $J = -16$ K (FM) for $U = 4.5$ eV and $J_H = 0.9$ eV (as were used, e.g., in $NaMn_7O_{12}$ [59] or in $Mn_4(hmp)_6$ [60]), which agrees with Goodenough-Kanamori-Anderson rules [30,53] but is inconsistent with experiment [53].

Thus, the results of the GGA calculations, where Li_2MnO_3 turns out to be a Slater insulator with the band gap appearing due to a spin splitting, seem to be reasonable. In the first order of the perturbation theory the exchange interaction in this situation is expected to be AFM. It can be described not by Eq. (14) but rather as

$$J \sim \frac{t_{dd}^2}{\Delta_{\mathrm{exc}}}, \tag{16}$$

where Δ_{exc} is the exchange splitting, which in the GGA is given by the sublattice magnetization M and Stoner parameter I as $\Delta_{\mathrm{exc}} = IM$ [61].

IV. CONCLUSION

We have presented the implementation of the Green's function approach for the Heisenberg model exchange parameters calculation. The localized electronic states were described by the Wannier functions with the symmetry of atomic orbitals. This basis set allowed us to overcome the limitations of modern plane-wave-based calculation schemes and perform a complex analysis of the intersite exchange interaction with the density functional theory or its extensions such as DFT+U. The results were tested on four transition metal compounds: NiO, FeO, $KCuF_3$, and Li_2MnO_3. The obtained values are in a good agreement with experimental estimations.

ACKNOWLEDGMENTS

We thank A. V. Lukoyanov and A. Pitman for valuable comments and J.-G. Park for the communications about layer A_2BO_3 compounds. The present work was supported by a grant from the Russian Scientific Foundation (Project No. 14-22-00004).

[1] D. Zakharov, H.-A. von Nidda, M. Eremin, J. Deisenhofer, R. Eremina, and A. Loidl, in *Quantum Magnetism*, edited by B. Barbara, Y. Imry, G. Sawatzky, and P. Stamp (Springer, Netherlands, 2008), NATO Science for Peace and Security Series, pp. 193–238.

[2] S. Blundell, *Magnetism in Condensed Matter*, Oxford Master Series in Condensed Matter Physics (Oxford University Press, Oxford, 2001).

[3] D. Khomskii, *Transition Metal Compounds* (Cambridge University Press, Cambridge, 2014).

[4] L. Noodleman, J. Chem. Phys. **74**, 5737 (1981).

[5] R. M. Martin, *Electronic Structure: Basic Theory and Practical Methods* (Cambridge University Press, Cambridge, 2004).

[6] A. A. Tsirlin, Phys. Rev. B **89**, 014405 (2014).

[7] A. Liechtenstein, V. Gubanov, M. Katsnelson, and V. Anisimov, J. Magn. Magn. Mat. **36**, 125 (1983).

[8] A. I. Liechtenstein, M. I. Katsnelson, V. P. Antropov, and V. A. Gubanov, J. Magn. Magn. Mat. **67**, 65 (1987).

[9] M. I. Katsnelson and A. I. Lichtenstein, Phys. Rev. B **61**, 8906 (2000).

[10] V. V. Mazurenko and V. I. Anisimov, Phys. Rev. B **71**, 184434 (2005).

[11] O. K. Andersen and O. Jepsen, Phys. Rev. Lett. **53**, 2571 (1984).

[12] F. Bloch, Zeitschrift für Physik **52**, 555 (1929).

[13] W. A. Harrison, *Elementary Electronic Structure* (World Scientific, Singapore, 1999).

[14] D. Singh, *Plane Waves, Pseudopotentials and the LAPW Method* (Kluwer Academic, The Netherlands, 1994).

[15] P. Giannozzi, S. Baroni, N. Bonini, M. Calandra, R. Car, C. Cavazzoni, D. Ceresoli, G. L. Chiarotti, M. Cococcioni, I. Dabo *et al.*, J. Phys.: Condensed Matter **21**, 395502 (2009).

[16] M. Methfessel and J. Kubler, J. Phys. F: Metal Phys. **12**, 141 (1982).

[17] N. Marzari and D. Vanderbilt, Phys. Rev. B **56**, 12847 (1997).

[18] I. Souza, N. Marzari, and D. Vanderbilt, Phys. Rev. B **65**, 035109 (2001).

[19] V. Anisimov, D. Kondakov, A. Kozhevnikov, I. Nekrasov, Z. Pchelkina, J. Allen, S.-K. Mo, H.-D. Kim, P. Metcalf, S. Suga *et al.*, Phys. Rev. B **71**, 125119 (2005).

[20] D. Korotin, A. V. Kozhevnikov, S. L. Skornyakov, I. Leonov, N. Binggeli, V. I. Anisimov, and G. Trimarchi, Eur. Phys. J. B **65**, 91 (2008).

[21] K. Momma and F. Izumi, J. Appl. Crystallogr. **44**, 1272 (2011).

[22] S. Hüfner, J. Osterwalder, T. Riesterer, and F. Hulliger, Solid State Commun. **52**, 793 (1984).

[23] B. E. F. Fender, J. Chem. Phys. **48**, 990 (1968).

[24] C. G. Shull, W. A. Strauser, and E. O. Wollan, Phys. Rev. **83**, 333 (1951).

[25] J. R. Tomlinson, L. Domash, R. G. Hay, and C. W. Montgomery, J. Am. Chem. Soc. **77**, 909 (1955).

[26] V. I. Anisimov, J. Zaanen, and O. K. Andersen, Phys. Rev. B **44**, 943 (1991).

[27] V. I. Anisimov, F. Aryasetiawan, and A. I. Lichtenstein, J. Phys.: Condens. Matter **9**, 767 (1997).

[28] J. P. Perdew and A. Zunger, Phys. Rev. B **23**, 5048 (1981).

[29] M. Hutchings and E. Samuelsen, Phys. Rev. B **6**, 3447 (1972).

[30] J. B. Goodenough, *Magnetism and the Chemical Bond* (Interscience Publishers, New York/London, 1963).

[31] K. I. Kugel and D. I. Khomskii, Soviet Physics Uspekhi **25**, 231 (1982).

[32] K. Kugel and D. Khomskii, JETP **37**, 725 (1973).

[33] A. Okazaki, J. Phys. Soc. Jpn. **26**, 870 (1969).

[34] A. I. Liechtenstein, V. I. Anisimov, and J. Zaanen, Phys. Rev. B **52**, R5467 (1995).

[35] J. E. Medvedeva, M. A. Korotin, V. I. Anisimov, and A. J. Freeman, Phys. Rev. B **65**, 172413 (2002).

[36] N. Binggeli and M. Altarelli, Phys. Rev. B **70**, 085117 (2004).

[37] J. P. Perdew, K. Burke, and M. Ernzerhof, Phys. Rev. Lett. **77**, 3865 (1996).

[38] K. Iio, H. Hyodo, K. Nagata, and I. Yamada, J. Phys. Soc. Jpn. **44**, 1393 (1978).

[39] S. Kadota, I. Yamada, S. Yoneyama, and K. Hirakawa, J. Phys. Soc. Jpn. **23**, 751 (1967).

[40] M. T. Hutchings, J. M. Milne, and H. Ikeda, J. Phys. C: Solid State Phys. **12**, L739 (1979).

[41] S. K. Satija, J. D. Axe, G. Shirane, H. Yoshizawa, and K. Hirakawa, Phys. Rev. B **21**, 2001 (1980).

[42] H. Fjellvg, F. Grnvold, S. Stlen, and B. Hauback, J. Solid State Chem. **124**, 52 (1996).

[43] D. G. Isaak, R. E. Cohen, M. J. Mehl, and D. J. Singh, Phys. Rev. B **47**, 7720 (1993).

[44] R. E. Cohen, I. I. Mazin, and D. G. Isaak, Science **275**, 654 (1997).

[45] A. O. Shorikov, Z. V. Pchelkina, V. I. Anisimov, S. L. Skornyakov, and M. A. Korotin, Phys. Rev. B **82**, 195101 (2010).

[46] J. Badro, V. V. Struzhkin, J. Shu, R. J. Hemley, H.-k. Mao, C.-c. Kao, J.-P. Rueff, and G. Shen, Phys. Rev. Lett. **83**, 4101 (1999).

[47] J. Zaanen, G. A. Sawatzky, and J. W. Allen, Phys. Rev. Lett. **55**, 418 (1985).

[48] V. Todorova and M. Jansen, Z. Anorg. Allg. Chem. **637**, 37 (2011).

[49] G. Jackeli and G. Khaliullin, Phys. Rev. Lett. **102**, 017205 (2009).

[50] S. A. J. Kimber, I. I. Mazin, J. Shen, H. O. Jeschke, S. V. Streltsov, D. N. Argyriou, R. Valenti, and D. I. Khomskii, Phys. Rev. B **89**, 081408 (2014).

[51] Y. Miura, Y. Yasui, M. Sato, N. Igawa, and K. Kakurai, J. Phys. Soc. Jpn. **76**, 033705 (2007).

[52] J. C. Wang, J. Terzic, T. F. Qi, F. Ye, S. J. Yuan, S. Aswartham, S. V. Streltsov, D. I. Khomskii, R. K. Kaul, and G. Cao, Phys. Rev. B **90**, 161110 (2014).

[53] S. Lee, S. Choi, J. Kim, H. Sim, C. Won, S. Lee, S. A. Kim, N. Hur, and J.-G. Park, J. Phys.: Cond. Mat. **24**, 456004 (2012).

[54] S. V. Streltsov and D. I. Khomskii, Phys. Rev. B **77**, 064405 (2008).

[55] I. Solovyev, N. Hamada, and K. Terakura, Phys. Rev. Lett. **76**, 4825 (1996).

[56] R. Weht and W. E. Pickett, Phys. Rev. B **65**, 014415 (2001).

[57] J. Park, S. Lee, M. Kang, K.-H. Jang, C. Lee, S. Streltsov, V. Mazurenko, M. Valentyuk, J. Medvedeva, T. Kamiyama *et al.*, Phys. Rev. B **82**, 054428 (2010).

[58] S. F. Matar, V. Eyert, A. Villesuzanne, and M.-H. Whangbo, Phys. Rev. B **76**, 054403 (2007).

[59] S. V. Streltsov and D. I. Khomskii, Phys. Rev. B **89**, 201115 (2014).

[60] S. V. Streltsov, Z. V. Pchelkina, D. I. Khomskii, N. A. Skorikov, A. O. Anokhin, Y. N. Shvachko, M. A. Korotin, V. I. Anisimov, and V. V. Ustinov, Phys. Rev. B **89**, 014427 (2014).

[61] V. Gubanov, A. Likhtenshtein, and A. Postnikov, *Magnetism and the Electronic Structure of Crystals* (Springer-Verlag, Berlin/Heidelberg, 1992).